The Cryosphere
Discussions

Open Access

EGU

Two-dimensional Inversion of wideband spectral data from the Capacitively Coupled Resistivity method - First Applications in periglacial environments

Jan Mudler[1], Andreas Hördt[1], Anita Przyklenk[1], Gianluca Fiandaca[2], Pradip Kumar Maurya[2], and Christian Hauck[3]

[1]Technische Universität Braunschweig, Institut für Geophysik und extraterrestrische Physik, Braunschweig, Germany
[2]Aarhus University, Department of Geoscience, Hydrogeophysics Group, Aarhus, Denmark
[3]University of Fribourg, Department of Geosciences, Fribourg, Switzerland

Correspondence: Jan Mudler (j.mudler@tu-bs.de)

Abstract. The Capacitively Coupled Resistivity (CCR) method determines the electrical resistivity and permittivity by analysing the spectra of magnitude and phase shift of the electrical impedance. The CCR is well suited for the application in cryospheric and periglacial areas, because these areas provide the required physical conditions and logistical advantages of the method regarding the problems of coupling on highly resistive grounds and in some cases hard surfaces. Since the electrical properties of

5   ice and frozen material have a strong frequency dependence, broad spectral measurements can deliver complementary information compared to conventional low-frequency techniques. For the inversion of the data, we modified an existing 2-D inversion code originally developed for low-frequency Induced Polarization data by including a Cole-Cole parametrization of electrical permittivity. We discuss the application of the code and particular aspects related to capacitively coupled measurements using data from two sites with cryospheric influence: the Schilthorn massif in the Swiss Alps and the frozen lake Prestvannet in the

10   northern part of Norway. We investigate the effect of capacitive sensor height above the surface and corroborate the assumption that it is negligible for highly resistive conditions. The first results agree reasonably well with known subsurface structure and measurements reported in the literature. We conclude that a spectral 2-D inversion with a Cole-Cole parametrization of permittivity is a feasible tool to invert CCR data in periglacial environments.

Copyright statement. TEXT

1   Introduction

15   Spectral electrical measurements over a wide frequency range allow the determination of the electrical resistivity ρ as well as the relative dielectric permittivity ε_r. The determination of the permittivity as an additional parameter can result in complementary information compared to conventional electrical measurements, which is useful for the interpretation of the subsurface conditions. Areas of low electrical conductivity are particularly suitable for the determination of both parameters. Ice or frozen

20   soils, such as permafrost, are potential fields of application, since they exhibit a characteristic frequency dependence of the

electrical impedance (Petrenko and Whitworth, 2002). In principle, the determination of the ice content in the subsurface is possible from the results of wide-band electrical measurements (Bitelli et al., 2004).

Many laboratory studies for the characterization of samples of frozen material were carried out (Olhoeft, 1977; Seshadri et al., 2008; Grimm et al., 2015; Murton et al., 2016; Zorin and Ageev, 2017). The first spectral measurements on ice and permafrost

5   at the field scale have been performed by Grimm and Stillman (2015) for a characterization of ice. Furthermore, the successful determination of the two electrical parameters at the field scale was demonstated by Przyklenk et al. (2016), using the method of Capacitively Coupled Resistivity (CCR). In contrast to galvanic coupling by skewers, in the case of CCR plates or cables lying on the ground are used, which are galvanically decoupled from the subsurface and guarantee purely capacitively coupling to the ground. This procedure may have several advantages under certain conditions. On the one hand, this method is non-invasive

10   and usable on extremely hard surfaces, such as rock or ice, on which it is hardly possible to work with skewers and often only by influencing the structure of the subsurface. Likewise, with the help of capacitive coupling, a coupling can be achieved even on subsoils of high resistivity (Hördt et al., 2013), on which galvanic coupling due to high contact resistivity is not possible, or only by special efforts at the electrodes. The CCR method is therefore not just useful for geophysical exploration on ice, but also for space missions (Grard, 1990; Grard and Tabbagh, 1991; Seidensticker et al., 2007) and for investigations in urban

15   areas such as facades (Souffaché et al., 2010) or roads (Dashevsky et al., 2005; Flageul et al., 2013) where prototypes were already used. Using capacitive coupling to the ground may be challenging, especially due to the sensor height effect, caused by effective height between the electrodes and the underlying subsurface. This could strongly influence the measurements and has to be considered (Kuras et al., 2006; Hördt et al., 2013).

Many studies which used the CCR method only measured the magnitude of the impedance at a discrete frequency and used the

20   method just like conventional resistivity measurements (Tabbagh et al., 1993; Kuras et al., 2007; Hauck and Kneisel, 2006). In order to be able to determine both parameters ρ and ε_r, additional measurements of the phase shift are required, which have to be carefully designed to avoid electromagnetic disturbances (Przyklenk et al., 2016). By measuring the values of amplitude and phase shift over a broad frequency range, it is possible to obtain the dielectric relaxation of the ground material. Based on a Cole-Cole parametrization of dielectric relaxation (Cole and Cole, 1941), an inversion for spectral measurements of CCR at

25   a single point using a homogeneous halfspace assumption was suggested by Przyklenk et al. (2016).

For the investigation of larger areas and depth, it is favorable to analyse data by a two- or even three-dimensional inversion. This is common for most geophysical methods, while for frequency-dependent measurements, existing 2-D inversions for conventional Spectral Induced Polarization (SIP) (Günther and Martin, 2016; Maurya et al., 2018) became available only recently. The aim of the present study is to investigate the applicability of the CCR method at the field scale in areas of surface (e.g.

30   lake ice) and subsurface (permafrost) ice occurrences. Two case histories will be discussed, one from the Schilthorn massif in the Swiss Alps and the other one from the frozen lake Prestvannet in the northern part of Norway. We modified the 2-D SIP inversion code in AarhusInv (Auken et al., 2014), an inversion tool for various geophysical methods, to consider the frequency-dependent permittivity in terms of a permittivity Cole-Cole model, and apply the code to the data of our two test sites. We also investigate the potential effect of electrode height and show that it is negligible in both cases. The results of the 2-D inversion

will be compared with existing knowledge about the subsurface stratifications and materials. We discuss the advantages of the determination of both electrical parameters and their potential for the interpretation.

2 Measurements and test sites

For the application of CCR, we focus on the cryosphere (i.e. ice, snow, permafrost), where the logistic advantages of the capacitive coupling are given in terms of highly resistive ground and in some cases hard surfaces (e.g. ice or frozen ground). The method enables the ability to measure directly on snow and ice. The measurements were carried out using the Chameleon equipment from Radic Research, which is specially designed for the application of broadband measurements of the electrical impedance (Radić, 2013; Przyklenk et al., 2016). The prototype device uses a 4-electrode array. Therefore, two-dimensional measurements along a profile and in depth are achieved by gradually shifting and enlarging the array. It is possible to measure in a range from $1 Hz$ up to $240 kHz$ at 19 discrete frequencies. The results are the spectral values of the magnitude $|Z(f)|$ and the phase shift $\varphi(f)$ of the impedance. Wenner- and dipole-dipole configurations were used.

2.1 Schilthorn

The survey was carried out in July 2016 on the Schilthorn massif, in the Bernese Alps, Switzerland. There is occurrence of alpine permafrost in the area, as documented by Hilbich et al. (2008) and Imhof et al. (2000). Figure 1 illustrates the geographical location. Panel B shows the area from village Mürren up to the summit Schilthorn. The mountain station Birg is in between and can be reached by a cable car. The position of the selected profile B-SCH, north of Birg, at an altitude of about $2700\,\mathrm{m}$ a.s.l. and with a length of 27 meters, is shown in Fig. 1C. The surface in this area mostly consists of rock, which is covered with snow most parts of the year (i.e. October-July).

The photograph in Fig. 2 shows an example of the equipment layout in the field. The plate electrodes, which are covered with capton foil for galvanic decoupling, were arranged in a profile line. They are connected by cables through a probe and a remote unit to the base unit (Przyklenk et al., 2016), which controls the measurements. The surface at the time of the measurements was covered by a layer of snow, which was frozen on the top. The depth of this snow layer was separately measured every two meters using a dipstick for later validation of the results. Measurements were done along the profile in a dipole-dipole configuration ($a = 1\,\mathrm{m}$) for several electrode spacings ($n = 1 - 6$).

2.2 Tromsø

The measurements in Norway were done in 2015 on the frozen lake Prestvannet near the town of Tromsø. Figure 3 shows the geographical position of the area and the test site. In Fig. 3B, a part of the peninsula Tromsøya, with the city Tromsø and the lake is visible. Lake Prestvannet covers an area of about 10 ha, has a maximum depth of 4 meters and is covered by ice most of the year (Stabbel, 1985). The part of the lake, where the test site is located, is shown in panel C, including the profile, which has an extension of 33 meters length and crosses the shore of the lake. The shore was covered with a layer of snow, the lake
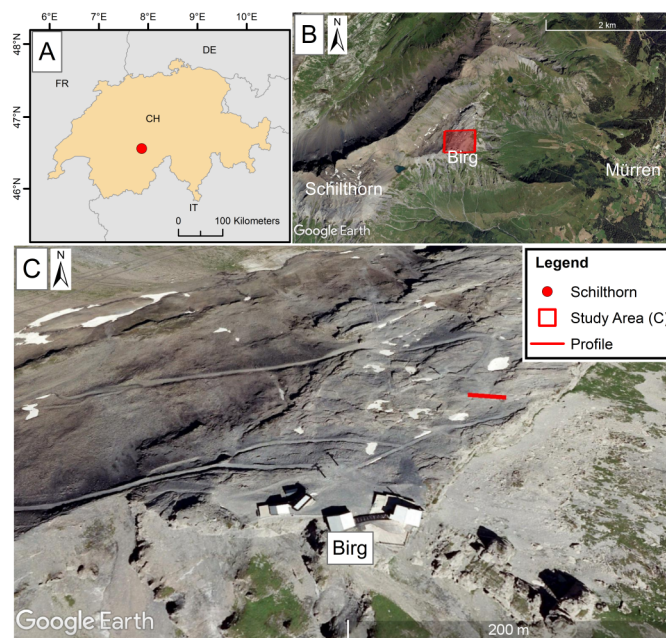
Figure 1. Geographical maps of the Schilthorn area. Panel A shows the location in Switzerland. In panel B the Schilthorn area with the village Mürren, the mountain station Birg and the summit is shown. The area around Birg, where the measurements took place is shown in panel C, including location of profile B-SCH.
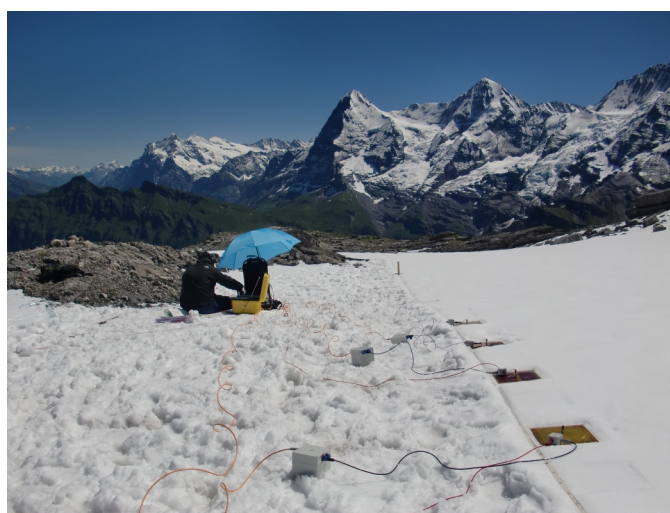

Figure 2. Photograph of the measurements at profile B-SCH (Schilthorn area) in July 2016 with the Chameleon measurement device. The four plate electrodes are lying in line on the snow surface. The larger yellow box is the base unit which is connected by cables to the electrodes with the cubic grey remote units in between.
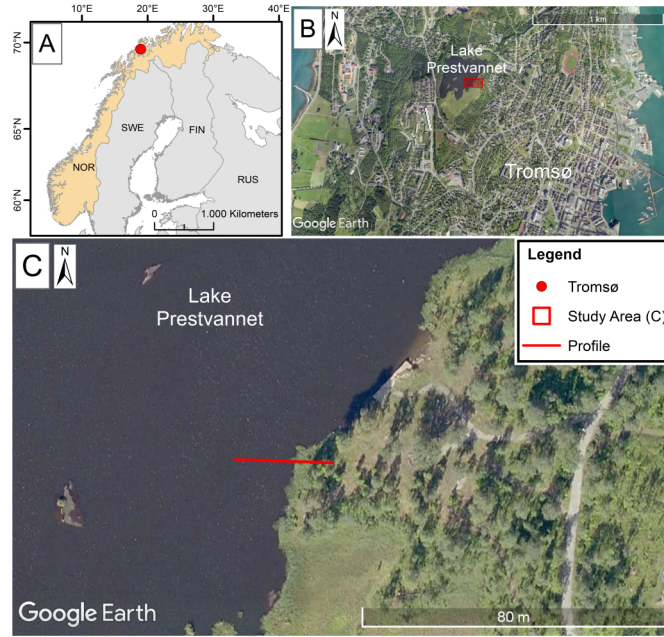
Figure 3. Geographical Maps of Lake Prestvannet. The location in the northern part of Norway is shown in part A by the red dot. The lake is located on the peninsula Tromsøya, presented in panel B, close to the city Tromsø. A detailed view of the test site is given in panel C, showing the profile crossing the boundary from the lake to the shore.

itself was frozen, and measurements took place directly on the lake ice. Starting the profile on the lake and ending at the shore, the transition to the lake surface is at about profile coordinate $20.5\,\mathrm{m}$.

The measurements were done with a fixed electrode spacing in Wenner configuration ($a = 1.5\,\mathrm{m}$) to investigate differences in the measured data due to the sub-vertical lake-shore-boundary. The penetration depth of the measurements has therefore a maximum of $1.5\,\mathrm{m}$ (Militzer and Weber, 1985). Additional measurements indicated that the boundary to the liquid water was at a minimum of $4\,\mathrm{m}$ depth, below the penetration depth of the data.

3 Basics of the Capacitively Coupled Resistivity Method

When a time-varying current is injected into the ground, two different physical mechanisms are stimulated: the conduction current associated with the electrical resistivity, and the displacement current controlled by the electrical permittivity. The response of the material contains a combination of these two mechanisms, which can be measured as the impedance. Consequently, it is possible to define an effective value named the complex conductivity, respectively the complex permittivity ε^*, which combines the conduction and polarization properties, as:

$$\varepsilon^*(\rho, \varepsilon_r, \omega) = \varepsilon_0 \varepsilon_r + \frac{1}{i\omega\rho}, \tag{1}$$

where i is the imaginary unit, ε_0 the permittivity of the vacuum and ω the angular frequency. Note, that the electrical resistivity ρ and the relative electrical permittivity ε_r are considered as real values. The three variable quantities, i.e. ω, ρ and ε_r determine in mutual dependence the weighting of the two current components. The injected current and the measured voltage are in-phase for the proportion of conduction current and shifted by $-90°$ for the displacement current component.

5　Most geophysical methods working with time-varying electric fields focus on one of the two mechanisms by defining a chosen frequency range and neglect the other part. The ratio of the proportions of both current mechanisms gives an estimation for the physical regime of the measurements. Geophysical methods such as Induced Polarization (IP) or Magnetotellurics (MT) (Telford et al., 1990) work in a rather low frequency range where the conduction current dominates the signal of the impedance. The Ground Penetrating Radar (GPR), on the other hand, works at very high frequencies and focuses on the displacement

10　current, determining the permittivity (Zorin and Ageev, 2017). Our aim is to measure in an intermediate frequency range where both current mechanisms are relevant in order to determine both electrical parameters (see Eq. (1)). In order to ensure this in our given frequency range, the subsurface materials have to exhibit relatively high resistivities and permittivities. The condition may be calculated based on the loss tangent (Przyklenk et al., 2016). Typically, for our frequency range the resistivity has to be greater than $1000\,\Omega\mathrm{m}$. The needed conditions are particularly prevalent in periglacial areas, where the occurrence of

15　ground ice can be relatively high (Arenson et al., 2015; Hauck and Kneisel, 2006).

In the early 1990s, the theory of a capacitively coupled quadrupolar array was first proposed by Grard (1990) and later deepened by Kuras et al. (2006). In the following years devices were developed and used in the field (Grard and Tabbagh, 1991; Tabbagh et al., 1993; Seidensticker et al., 2007; Kuras et al., 2007). The assumption is that the galvanically decoupled electrodes in the form of plates, disks or wires are lying on the interface between two media. In most cases, and in the following considerations,

20　it is the interface between air and ground. The theory leads to a description of the complex impedance as follows, where the form suggested by Kuras et al. (2006) was modified by Przyklenk et al. (2016) in order to use the unmodified geometry factor K, known from DC resistivity:

$$Z(\omega, \rho, \varepsilon_r, h) = \frac{1}{2i\omega\varepsilon_0 K}[1 - \alpha(\rho, \varepsilon_r)H(h)], \tag{2}$$

25

where the reflection factor α contains both electrical parameters of the subsurface.

Special attention is given to the height factor $H(h)$. It depends on the geometry factor K and a vertical geometry factor, which describes the height of the capacitively coupled sensors. In the case of an ideal contact of the electrodes to the ground, the height h becomes zero and the resulting height factor H becomes one. Thus, the electrical parameters for each frequency can

30　be determined directly from the real and imaginary part of the impedance (Przyklenk et al., 2016):

$$\rho = \frac{K}{Re(Z^{-1})} \tag{3}$$

6

$$\varepsilon_r = \frac{Im(Z^{-1})}{K\omega\varepsilon_0} - 1 \tag{4}$$

The challenge is that the electrodes, especially in the case of plates or discs usually do not rest over their entire surface on the
ground. Rather, with a slight unevenness of the ground, a contact of the electrodes to the ground is ensured only at a few points.
This results in a mean non-zero height h of the electrode surface over the ground, which however can hardly be measured
directly. The height dependence was already discussed by a few authors (Kuras et al., 2006; Przyklenk et al., 2016). Even small
heights in the range of micrometers can cause large differences in the measured impedance, but this dependence becomes
weaker as resistivity and permittivity increase.

3.1 Cole-Cole Model

The electrical permittivity and the resistivity are not constant values in most cases but vary with frequency. Polarizable materi-
als, e.g. water-saturated sediments or mineralized rocks exhibit a strong frequency dependence of electrical parameters (Zorin
and Ageev, 2017). This is especially true in periglacial areas, for materials with pure ice or large ice contents (Petrenko and
Whitworth, 2002; Bitelli et al., 2004; Stillman and Grimm, 2010). Przyklenk et al. (2016) investigated several parametrizations
of the frequency-dependence of resistivity and permittivity. They suggest the use of the Cole-Cole Model (CCM) (Cole and
Cole, 1941), which provides reasonable results when fitting the spectral data of CCR measurements. For variable data with
more spectral shape, a dual CCM, corresponding to a model of a two-component mixture, might be necessary for the evaluation
of the impedance spectrum. For our studies, we decided to use the single CCM, which includes just one material, because it
can fit our data with a minimum number of parameters. For the relative complex permittivity, the single Cole-Cole Model is
expressed by:

$$\varepsilon_r^* = \varepsilon_{HF} + \frac{\varepsilon_{DC} - \varepsilon_{HF}}{1 + (i\omega\tau)^c} + \frac{1}{i\omega\varepsilon_0\rho_{DC}}. \tag{5}$$

The description of the frequency dependence of the electrical parameters is based on five Cole-Cole parameters: the DC
resistivity ρ_{DC}, a low-frequency limit ε_{DC}, a high-frequency limit ε_{HF}, which is referred in the literature as the dielectric
constant, the relaxation time τ and the relaxation exponent c. The positive relaxation exponent can range up to a maximum
value of one, for which the model simplifies to the Debye Model (Petrenko and Whitworth, 2002). Except for the relaxation
exponent, all values are material-specific parameters for which ranges of literature values are known, that can be used for a
discussion of the inversion results.

3.2 Single Site Inversion

The single site inversion was the primary method used in Przyklenk et al. (2016). The data of each measured 4-point array is inverted separately, i.e. without influence of other measurements. Thus, this spectral inversion contains a dependence on frequency, but not on space. In this context it is important to note that under the physical conditions of the CCR method,

5 the propagation of the electromagnetic fields is just limited by the geometry but not by the used frequency (Weidelt, 1997). Induction effects can be neglected in case of high resistive environments and small electrode distances (Fiandaca, 2018). Thereby, the penetration depth of the measurements is only controlled by the geometric size of the configuration, i.e. the geometry factor K, in contrast to the frequency sounding where the frequency dependent skin depth describes the penetration depth (McNeill, 1980).

10 The fit of the measured spectral data of the magnitude $|Z(f)|$ and phase shift $\varphi(f)$ is done under parametrisation of the complex impedance (Eq. (2)) by the single Cole-Cole Equation (Eq. (5)). The inversion is based on the model of a homogeneous halfspace. From the result of the inversion, the five Cole-Cole Model parameters can be extracted. Moreover, the single site inversion has the possibility to take the sensor height effects into account. By using the mean electrode height h as an additional free inversion parameter, it is possible to include the effect of electrode height and at the same time determine its value.

15 Thereby, capacitively coupled measurements taken under conditions of strong height influence, in particular on low resistive subsurfaces, can also be evaluated. If the height is neglected during inversion, this can in principle lead to a distortion of the data and erroneous results. Since in the next step we use a conventional 2-D inversion code for spectral IP data, where the height effect is not included into the forward modelling, it is essential to test whether it is justified to neglect it. For this purpose, we carry out the single site inversion twice: first including the height effect by setting the height as a free parameter and once under

20 the assumption of no sensor height, i.e. by fixing it to zero.

Figure 4 shows a representative example of the spectra for magnitude (a) and phase shift (b) from a measurement at profile B-SCH. The points indicate the measured data, the lines are the calculated spectra for the best-fit model. Inversion is done with (CCM h_{inv}) and without (CCM h_0) determination of height. The calculated height for CCM h_{inv} is $7 \cdot 10^{-7}\,\mathrm{m}$. This is so close to zero that the results exhibit no visible difference in the measured frequency range. The parameters of the Cole-Cole Model,

25 given in the caption of the Figure, have no difference if rounded to a maximum of two decimal places.

The magnitude adopts a value of around $2 \cdot 10^5\,\Omega$ for low frequencies, where the curves converge to a constant value. The phase shift covers almost the entire range that is theoretically possible (0 to $-90°$). The values close to zero for low frequencies indicate a domination of conduction currents, whereas the deviation from zero for increasing frequencies indicates the increasing relevance of displacement currents. It is expected that for higher frequencies out of the measured range, the phase

30 shift approaches the limit of $-90°$ where displacement currents dominate. The aim of measuring the intermediate range with the transition between both current mechanisms has been achieved in this case. The measured spectral signals in Fig. 4 are typical of the whole measurements on the profile. The values of magnitude are decreasing for larger configurations because of the increasing geometry factor. The phase shift shows the characteristic wavelike shape with a local minimum and maximum. The data fit of the single site inversion is reasonable, justifying the usage of the single Cole-Cole Model.
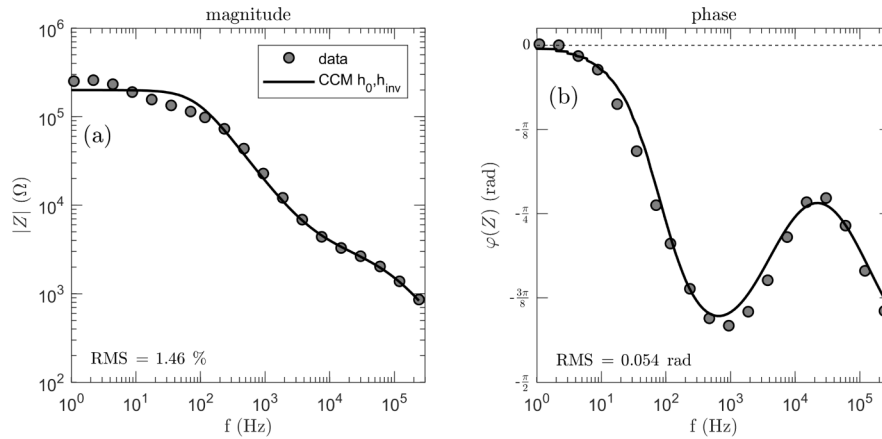
Figure 4. Spectra for the magnitude (a, left) and the phase shift (b, right) of the impedance for measured data (dots) and inversion results by using the Cole-Cole Model (CCM, lines). The inversion was carried out twice, with the assumption of zero electrode height (h_0) and by calculating the height as an additional inversion parameter (h_{inv}). The simulated curves of the two inversions can not be distinguished from each other. Data were measured at profile B-SCH, Schilthorn area, Switzerland, in a dipole-dipole configuration ($a = 1m$, $n = 1$). The CCM parameters are (h_0 and h_{inv}): $\rho_{DC} = 3.8 \cdot 10^6\,\Omega\text{m}$, $\varepsilon_{DC} = 53$, $\varepsilon_{HF} = 2.8$, $\tau = 3.6 \cdot 10^{-5}\,\text{s}$, $c = 0.82$.

In case of Lake Prestvannet we assume a sub-vertical separation through the measurements over the lake shore. Two representative signals are shown in Fig. 5 to illustrate the difference between the characteristic curve shapes. The magnitude exhibits a stronger frequency dependence in case of the land measurements and a higher value for low frequencies of about one order compared to the lake measurements. For the phase shift, the shape of the curve measured on the lake is flatter and the local

5 minimum is at higher frequencies. The phase shift shows smaller dynamics for the lake than for the land measurements. The Figure illustrates that the different ground materials provide significant differences in their response.

The inversion was done with and without including the determination of sensor height. For the onshore measurement the estimated height is $2.5 \cdot 10^{-5}\,\text{m}$, which results in no visible difference between the simulated curves. For the lake measurement the fitted height of $1.2 \cdot 10^{-3}\,\text{m}$ leads to a visible difference for the phase shift (panel b). The two calculated spectra vary for

10 the lowest frequencies. While the inversion with zero height (continuous line) converges towards zero, the version including height (dashed line) shows a deviation from zero consistent with the data. The data fit shows a difference also in terms of the root mean square (RMS) which is better for CCM h_{inv}. It is known from theory that the height dependence has stronger effects for lower frequencies and is stronger for the phase than for the magnitude of the impedance (Przyklenk et al., 2016). Our data, with a visible effect in the phase shift and negligible effect in the magnitude for the data set with the smaller impedance (panel

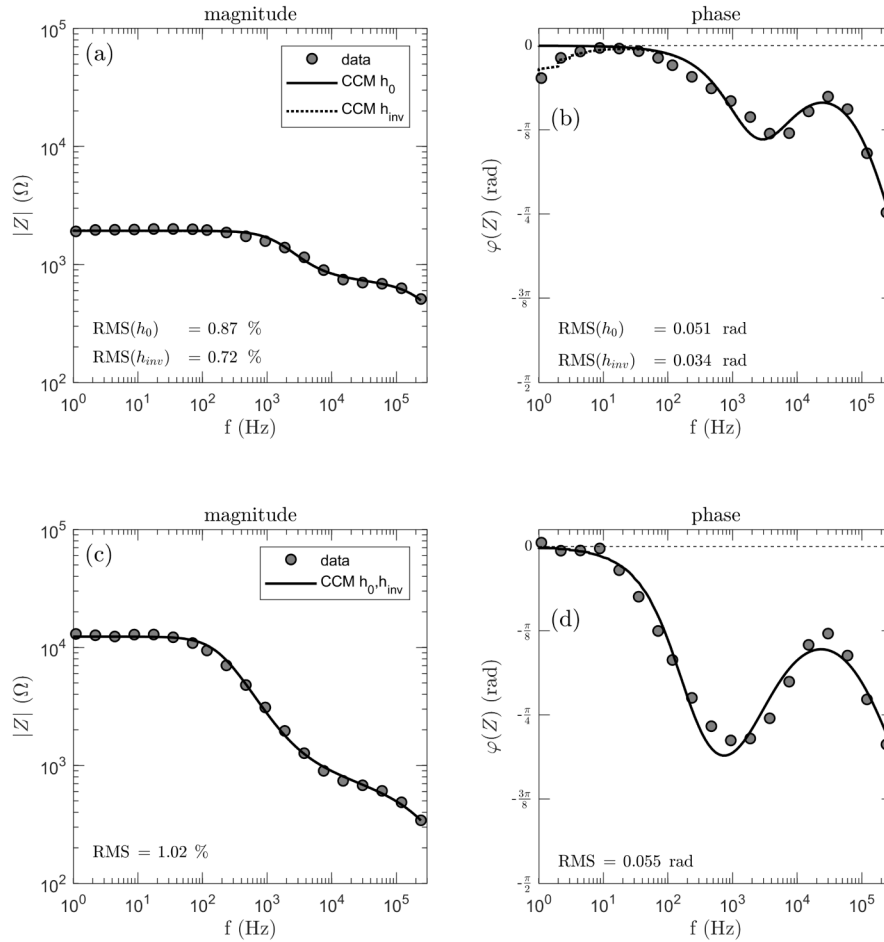15 a,b) is consistent with these theoretical results.

Figure 5. Spectra of two measurements from the Tromsø site. Panel (a,b) show data from the lake and panel (c,d) data from a measurement on shore. The figure shows the measured data and the inversion results using the Cole-Cole Model. The simulated curves with zero electrode height (h_0) and inverted height (h_{inv}) can not be distinguished, except for the phase shift of the lake measurement (panel b). Both measurements were taken with a Wenner-configuration with $a = 1.5$ m.

The CCM parameters for the lake measurement are (h_0/h_{inv}): $\rho_{DC} = 1.82 \cdot 10^4/1.81 \cdot 10^4 \, \Omega$m, $\varepsilon_{DC} = 374/370$, $\varepsilon_{HF} = 8.80/8.83$, $\tau = 4.2 \cdot 10^{-5}/4.1 \cdot 10^{-5}$ s, $c = 0.93/0.93$.

The CCM parameters for the onshore measurement are (h_0 and h_{inv}): $\rho_{DC} = 1.2 \cdot 10^5 \, \Omega$m, $\varepsilon_{DC} = 670$, $\varepsilon_{HF} = 12.8$, $\tau = 7.1 \cdot 10^{-5}$ s, $c = 0.84$.
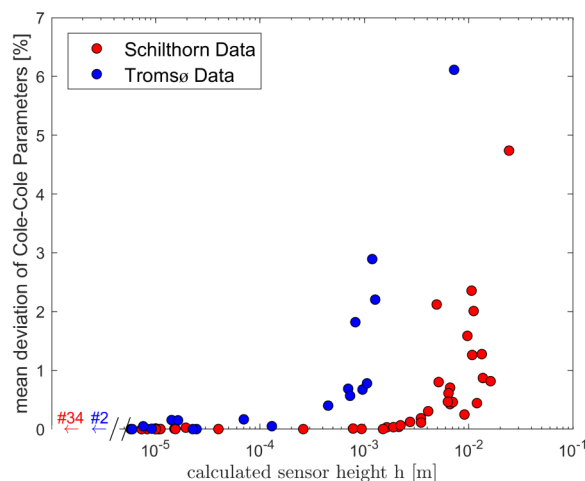
Figure 6. Mean deviation of Cole-Cole parameters vs. sensor height. The deviation was calculated by performing the single site inversion with and without the determination of sensor height and calculating the ratio for all the five Cole-Cole parameters. The data are separately shown for all measurements at profile B-SCH (Schilthorn, red) and Lake Prestvannet (Tromsø, blue). Values for sensor heights lower than $5 * 10^{-6}$ m are not displayed but their number of measurements is shown.

3.3 Influence of Electrode Height on Cole-Cole Parameters

In the following, we analyse the dependence of the Cole-Cole parameters on the electrode height in some more detail. The reason is, that the 2-D inversion used later is not able to consider non-zero electrode height. Therefore, the single site inversion was performed for every measured array of both field areas in both versions, with and without determining h. For every

5 array, the five resulting Cole-Cole parameters were put into relation for both inversions and the mean deviation in percent was calculated. This deviation is shown in dependence on the estimated sensor height in Fig. 6.

For larger sensor height, the Cole-Cole results are more affected. The Schilthorn data (red dots) show a strong increase of deviations from approximately $5 \cdot 10^{-3}$ m height on, where for the Tromsø data (blue dots) this increase occurs for sensor heights about one order of magnitude lower. The different behaviour can be explained by the condition of lower electrical

10 resistivities for the Tromsø measurements. As mentioned earlier, the height effect is stronger for lower ground parameters of resistivity and permittivity. Furthermore, for the Schilthorn data higher values of sensor height were determined. This could indicate that in case of the solid ice surface, as on the lake, the contact of electrodes to the ground is very smooth, resulting in a more homogeneous sensor height. On the other hand, the snow surface at Schilthorn builds a more porous ground. The loose material might cause a poorly defined contact and lead to an artificially increased apparent electrode height. The Schilthorn

15 data shows scattered sensor heights, which indicates the uncertainty in the electrode contact surface. It should be noted that the calculated sensor height in Fig. 6 are shown only down to the lowest values of $5 \cdot 10^{-6}$ m, but also lower values were determined. Investigations from Przyklenk et al. (2016) and Kuras et al. (2006) indicate that electrode heights lower than

11

around 10^{-4} m do not effect the measured signal, especially under high resistive conditions. Smaller heights determined by the inversion are mainly caused by numerical reasons and does not represent physical conditions. They can be seen as equal to zero. The determined values of the Schilthorn measurements range from less than 10^{-9} m up to centimeters. On the other hand the Tromsø results only vary from 10^{-7} m to the millimeter range.

5 Additional investigations, which will not be further elaborated here, have indicated that the parameters ρ, ε_{DC} and τ are generally more affected than ε_{HF} and c. That is consistent to the fact that the electrode height effects mainly the lower frequencies. All in all, the deviations of the Cole-Cole results are relatively small. Except for the two highest values in Fig. 6, their effect is smaller 3 percent. These deviations are considered to be acceptable, compared to the typical Cole-Cole parameter resolution for inversions (Yuval and Oldenburg, 1997; Madsen et al., 2017). The results justify therefore the use of inversions

10 without considering effective sensor height, as in the case of the 2-D inversion (see next section). It should be noted that under less favourable conditions, depending on the electrical parameters of the soil and the texture of the surface, neglecting the height can lead to larger errors. Neglecting height is therefore not a general recommendation, but has to be investigated separately for each application with different subsurface conditions. In the case of snow or icy ground, one additional benefit is that these are rather smooth surfaces, where the electrode height is small. On uneven surfaces, such as gravel and rock fields,

15 an installation of the plate electrodes without height variations may be difficult to achieve.

4 2-D Inversion with AarhusInv

The full spectral inversion of complex resistivity data, where all frequencies are being inverted simultaneously, has been a challenge for some time. For example, Grimm and Stillman (2015) used a workaround based on the time-lapse feature of RES2DINV (Loke and Barker, 1996) to invert their broadband SIP data from a periglacial environment. Recently, a few

20 codes for full spectral inversion have become available (Günther and Martin, 2016; Maurya et al., 2018). Here, we use the program AarhusInv (as in Maurya et al. (2018)), which is a tool for the inversion and modelling of geophysical data for several measurement methods (Auken et al., 2014). In AarhusInv the complex impedance is modelled in 2-D solving the Poisson's equation, Fourier transformed in the strike direction, without considering EM effects (Fiandaca et al., 2013). All the inversion parameters are inverted simultaneously using all the measured frequencies in a unique inversion process (equivalently to the

25 spectral full-decay inversion of the time-domain IP data). In case of Induced Polarization, where the frequency range is usually only up to one kilohertz, in general relatively small phase shifts are measured. In order to use the inversion for the CCR method, we included the permittivity Cole-Cole Model defined by Eq. (5) to parameterize the frequency-dependent electrical properties. Compared to the conventional Cole-Cole resistivity model that is defined by four parameters and is sometimes used to parameterize low-frequency SIP spectra (Pelton et al., 1978; Tarasov and Titov, 2013), the model defined by Eq. (5) has

30 one more parameter, basically corresponding to the high-frequency limit of permittivity. Therefore, the result of the inversion is a distribution of the five Cole-Cole parameters. As discussed previously, the height of the electrodes is not included into AarhusInv and assumed to be zero. Through this approximation the application for CCR data is usually just suitable under highly resistive conditions. Of course, this inversion method could generally be used for high frequency spectral resistivity

measurements, including galvanically coupled electrodes.

In the following, we will show the results of the 2-D inversion for both field sites. The resulting distribution of all Cole-Cole parameters will be discussed and compared with the expected properties of the subsurface.

4.1 Schilthorn

The measured data from profile B-SCH were evaluated by the 2-D inversion. The result is shown in Fig. 7, where several 2-D models for the five Cole-Cole parameters ρ, ε_{DC}, ε_{HF}, τ and c are shown color-coded vs. depth and horizontal coordinate. The dashed black line corresponds to the manually measured depth of the top snow layer. The brighter areas are those below a depth of investigation value (DOI), areas where the parameters can no longer be reliably estimated. The calculation of the DOI was described in Fiandaca et al. (2015). This boundary differs for each parameter, having in most cases the deepest extent for the resistivity model. This suggests that resistivity is better constrained than the other parameters. It should be noted that the measurements were not carried out with the same electrode spacing throughout the profile. Measurements with wider electrode spacing and corresponding larger penetration depth were carried out only on the first half of the profile.

First, we focus on the structural aspects of the results. The structure is a little different for each of the five sections, but in general a structure of two layers can be recognized, representing the top snow layer and the underlying surface layer. Because of the additional snow depth measurements, the results of the inversion can be validated. Especially for ε_{DC}, the boundary of the snow layer agrees well with the corresponding parameter contrasts. Around profile meter 20, where the boundary indicates a ditch, it becomes particularly clear how precisely the layer structure is reflected by the low-frequency permittivity value (panel b). The layer boundary can also be seen from the result of the resistivity (panel a), where a highly resistive surface layer is followed by a more conductive material. Unlike in the ε_{DC} section, there is a continuous decrease in the value with the depth, which makes the layer transition appear more smoothly. The layer boundary is also apparent in the section of parameter τ (panel d). The relaxation exponent c (panel e) also indicates the boundary. In the lower layer, c is close to 1, corresponding to a Debye relaxation. Compared to the other parameters, less literature is available for the relaxation exponent and the values are close to each other. Therefore, c seems less suitable for an interpretation in terms of material properties. The high frequency value ε_{HF} (panel c) is the only one which does not show a clear distribution. The range in this case is significantly smaller compared to the other parameters, which could make it more difficult to identify differences in materials based on ε_{HF}. This is the case in this example but could be different for other test sites or under different condition. The region of slightly higher values at about two meter depth on the second half of the profile could indicate a systematic change in the permittivity.

The two layers could be identified as the snow layer and the underlying bedrock, expected as limestone layer described by Rowan (1993), which could also be seen at some spots on the surface near the profile area. The resistivity and the relaxation time on the first half of the profile show some more variation underneath the snow, possibly caused by a third layer of weathered material on top of the bedrock. It is unclear whether the layer of limestone or possible weathered material under the snow is frozen or unfrozen. For the time of measurements the subsurface is usually unfrozen, but as the snow cover isolates the ground, the subsurface could be slightly frozen.

The determined values in their dominating range for the two horizontal regions of profile B-SCH are compared to literature in
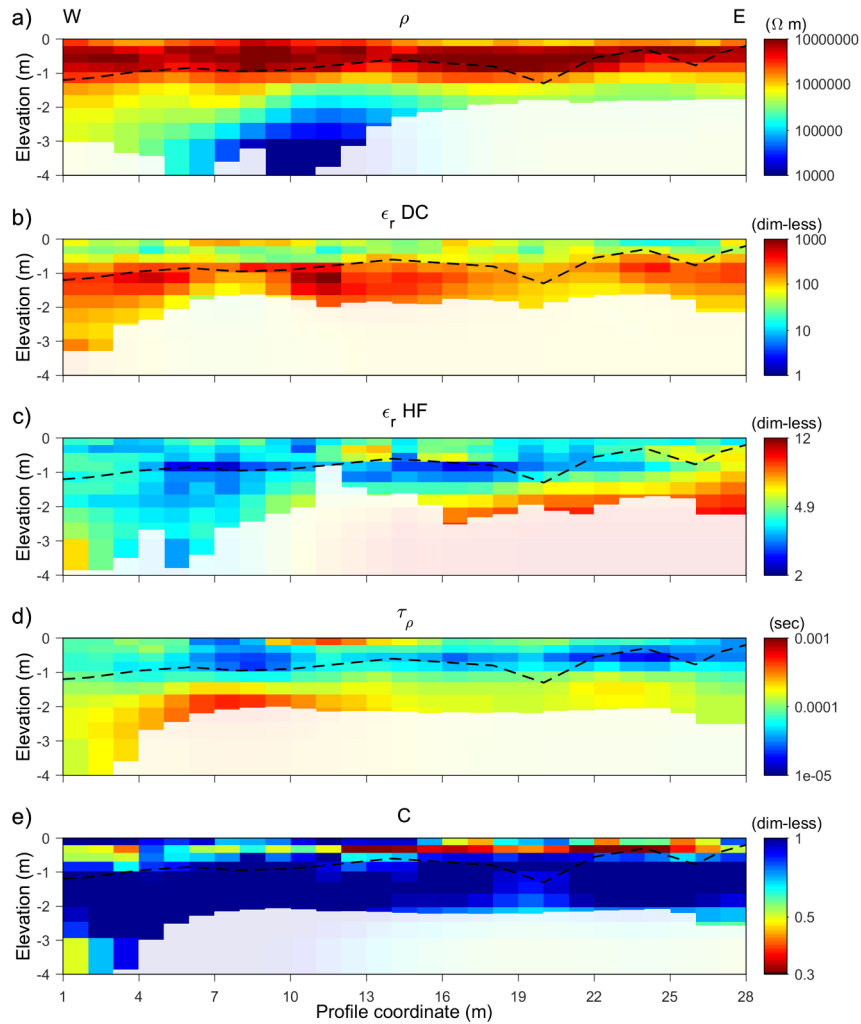
Figure 7. Result of the AarhusInv 2-D inversion for the data from the Schilthorn area along the profile B-SCH denoted in Fig. 1. The figure shows the sections of the five Cole-Cole parameters (a-e) defined by eq. (5). The dashed line shows the separately measured depth of the snow-layer, the brighter parts represents the area where the depth of investigation is exceeded.

table 1. The literature values of the different materials can vary over large ranges, which is mainly caused by the differences in physical conditions. For ice and snow the purity, density, salinity and temperature can strongly influence the electrical parameters (Arenson et al., 2015; Evans, 1965). New and soft snow, as it was present in case of the Profile B-SCH, has a relatively low density, meaning an increase of resistivity towards more dense snow. For the literature values of ice the attribute pure means that there is no impurity caused by other materials in the ice/water, but there are still variations based on the physical conditions like temperature. If ground material is frozen, like on permafrost or seasonal frost, the measured signal is expected to react as a composition of the basic material and ice (Zorin and Ageev, 2017). The parameters for frozen ground

Table 1. Results of the 2-D inversions on profile B-SCH and the profile on Lake Prestvannet and comparison with literature values for snow, ice, water and limestone, which is expected as bedrock material on B-SCH. The characteristic parameters from the inversions are given as the range for the two horizontal layers for profile B-SCH and the two vertical separated regions of lake and shore for the profile on the Lake Prestvannet. Literature values were taken from Arenson et al. (2015)[1], Evans (1965)[2], Achammer and Denoth (1994)[3], Palacky (1988)[4], Murton et al. (2016)[5], Olatinsu et al. (2013)[6] and Seshadri et al. (2008)[7].

		$\rho_{DC}[\Omega m]$	$\varepsilon_{DC}[-]$	$\varepsilon_{HF}[-]$	$\tau[s]$
B-SCH	First Layer	10^6 - 10^7	15 - 100	2 - 9	10^{-5} - 10^{-4}
	Second Layer	10^3 - 10^6	50 - 700		10^{-4} - $5 \cdot 10^{-4}$
Lake Prestvannet	Lake	10^4 - $2 \cdot 10^4$	750 - 3000	5 - 11	10^{-4} - $6 \cdot 10^{-4}$
	Shore	$4 \cdot 10^5$ - 10^4	850 - 6500	12 - 15	$6 \cdot 10^{-5}$ - $2 \cdot 10^{-4}$
Literature	Snow[1,2,3]	10^5 - 10^8	~ 40	< 15	$\sim 10^{-4}$
	Limestone (unfrozen/frozen)[4,5,6]	10^3 - 10^5	50 - 130	5 - 9	$2 \cdot 10^{-5}$ - $> 10^{-4}$
	Ice (pure)[2,7]	10^5 - 10^9	92 - 105	3	10^{-4} - $5 \cdot 10^{-3}$

are strongly dependent on the ice content and temperature (Arenson et al., 2015; Grimm et al., 2015). In the case of limestone, laboratory investigations of CCR by Murton et al. (2016) showed, that the resistivity of a frozen limestone sample ($10^5 \, \Omega\text{m}$) can be one magnitude higher than for the same sample in an unfrozen state.

In summary, the determined Cole-Cole parameters from the 2-D inversion are consistent with the literature values for the expected materials. The parameters of the top layer correspond to the values of snow. For the underlying layer, the literature for limestone are in agreement with the estimated values. The further separation in resistivity could be caused by a frozen state, which should increase the value of pure limestone, or could be caused by general differences in material.

A comparison with the results of the single site inversion illustrates the differences of the inversion methods. Figure 8 shows the results for the same measurements as in Fig. 7 but evaluated by the single site inversion. The parameters are determined individually for each quadrupolar measurement. In order to represent the results in a two-dimensional structure, the results are assigned to a certain location according to the midpoint position and extent of the array. Thus, a two-dimensional pseudo-section is finally created for each parameter, which can provide a rough overview of the subsurface structure. One has to keep in mind, that the pseudo-sections in Fig. 8 show inverted data and not just measured data as it is for example in the case of DC resistivity measurements. As expected when comparing pseudo-sections with 2-D inversion results, overall structures are similar, but there are differences in detail. The low-frequency permittivity (panel b) and the relaxation time (panel d) systematically increase with depth, while the resistivity (panel a) shows a decrease with depth, all indicating a horizontally layered structure. As seen before in the 2-D results, the high permittivity value ε_{HF} exhibits a small range of values and does not show a systematic distribution, but fits in the range of the literature. Since the results of the deeper pseudo-layers always represent an integral value over the entire depth range, it has to be expected that clear boundaries between the layers can not be identified by this method. Therefore the measurements have to be analysed in dependence to each other, as it was done by the
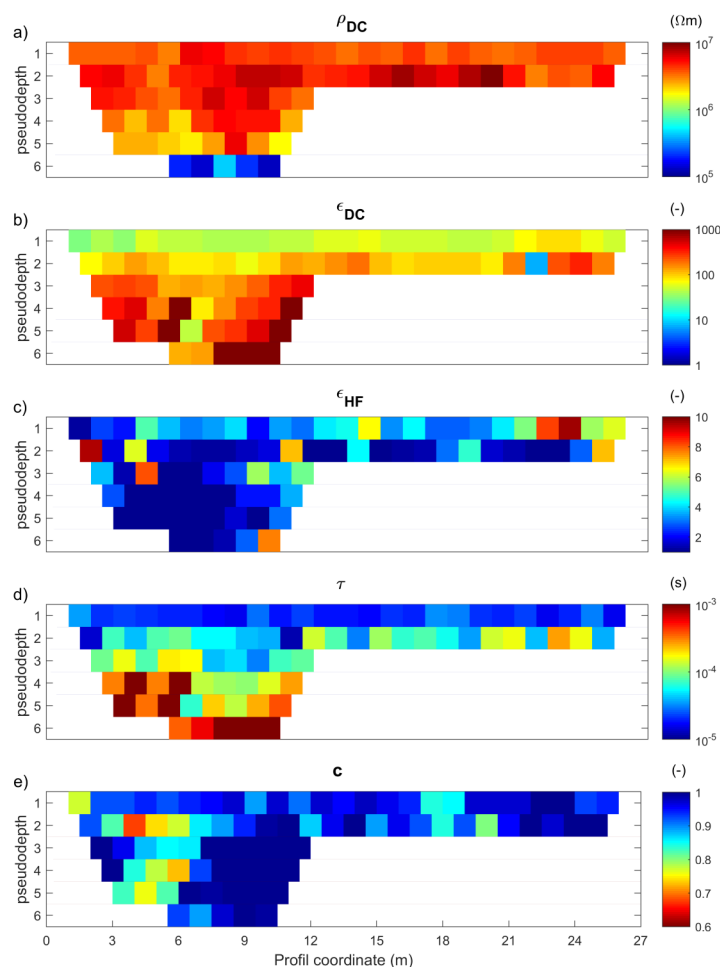
Figure 8. Pseudosections of the five Cole-Cole parameters (a-e) calculated by the single site inversion for profile B-SCH. Measurements were done for larger configurations on the left half of the profile.

2-D inversion. However, since the inversion with respect to the frequency dependence is independent for the two methods, we take the qualitative consistency as evidence that our 2-D inversion is a feasible tool to invert spatial and frequency dependence at the same time.

4.2 Tromsø

5   The investigations at Lake Prestvannet focus on the vertical transition from the lake to the shore rather than on the distribution with depth. In Fig. 9, the result of the AarhusInv 2-D inversion is shown for all Cole-Cole parameters. Measurements were
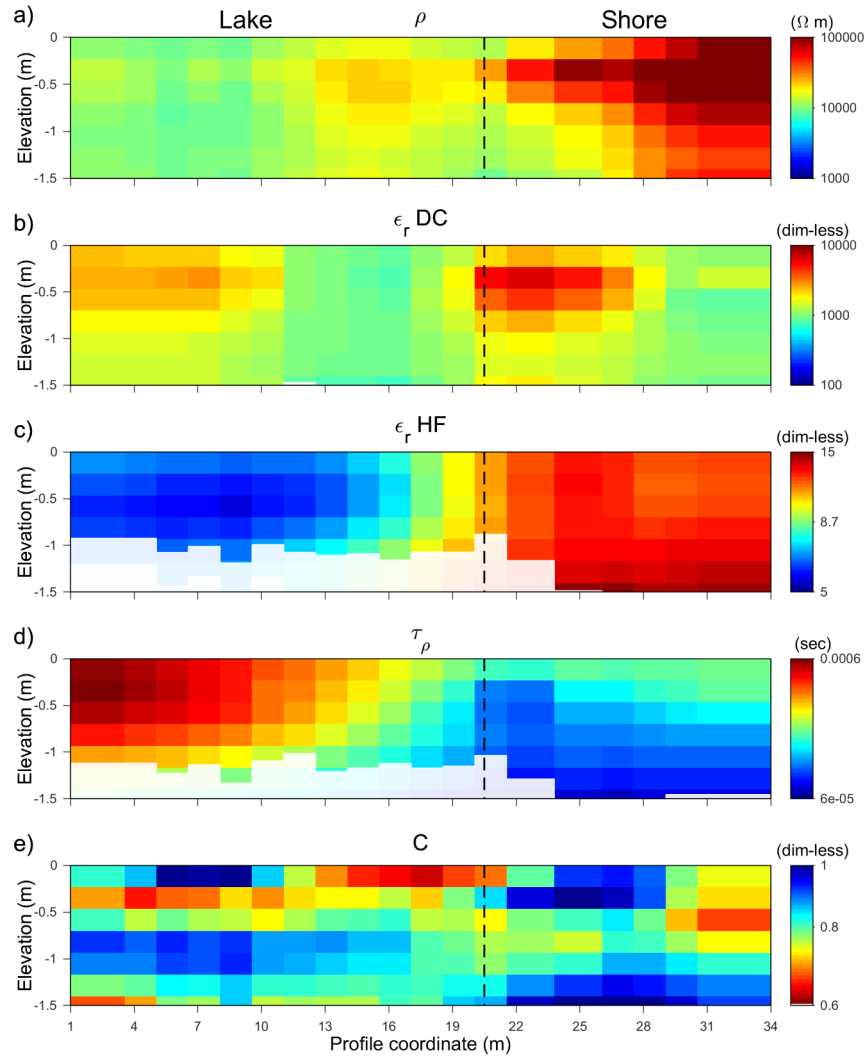
Figure 9. 2-D inversion result of the 5 Cole-Cole parameters (a-e) for the measurements at the lake Prestvannet denoted in Fig. 3. The surface boundary between lake and shore is at profile meter 20.5, indicated by the dashed line, where a change in most parameters can be recognized. The whitened areas are those where the value of DOI is exceeded.

carried out for just a small spacing (Wenner $a = 1.5\,\mathrm{m}$), so the penetration depth is not more than approximately 1.5 meters. Brighter areas are again below the DOI and the vertical black line indicates the surface position of the transition from the lake to the shore at profile meter 20.5. Except for the relaxation exponent c (panel e), in all models the transition is defined by a parameter change. The ranges of the estimated Cole-Cole parameters for lake and shore are given in table 1 and can be compared to the literature values of snow and ice.

5

The high-frequency permittivity ε_{HF} (panel c) shows lower values for the lake than onshore. This parameter is somewhat specific, because the variation from lake to shore is the only prominent variation, whereas the other parameters also show some structure within both sides. Compared to profile B-SCH (Fig. 7), where ε_{HF} has a small dynamic range with little spatial coherence, for the data of Lake Prestvannet both permittivity values ε_{DC} and ε_{HF} seem to be useful to distinguish different

5   materials or the state of freezing. The low-frequency permittivity ε_{DC} (panel b) shows the transition from lake to shore, but exhibits additional variation on either side of the transition. The land side shows an anomaly close to the transition. The cause is not exactly known, but we hypothesize that it indicates a change in sediments. A detailed analysis, where the two properties of permittivity may be combined with resistivity in a multi-parameter analysis may be a subject of future research. The relaxation time τ shows relatively homogeneous values for each of the sides. The fact, that the relaxation times of snow are shorter than

10   those of ice (Evans, 1965) is consistent with our results. The resistivity ρ_{DC} decreases from higher values on the snow covered land side, by about one order of magnitude on the lake. The relaxation exponent c shows small variations and poor spatial coherence, and is difficult to interpret in terms of material variations.

Onshore, the measurements were taken on the snow and the known values of snow are consistent for some parameters. Higher density of the snow could explain the much lower resistivity than obtained for the snow at B-SCH. However, in combination

15   with the values of ε_{DC} which are higher than expected for snow, this could indicate that the measurements are under the influence of the ground material beneath. For the frozen lake, the values estimated from the inversion are a bit higher than typical literature values for ice. However, it is known that the electrical parameters of frozen water bodies can be very different from those of pure ice. The lake ice could be a composition of ice and partly water, insteat of a pure ice body. Such mixtures can result in much higher values of permittivity, because water has a value ε_{HF} of about 80 (Evans, 1965). Lower values of

20   resistivity could as well be explained by this composition because water has a lower intrinsic resistivity than ice. A similar observation was made by Przyklenk et al. (2016) during their discussion of measurements on mountain ice.

4.3   Data fit

For the assessment of the inversion results, we consider their quality in terms of the data fit. Because of being a spectral inversion, the inversion includes the fit of all measured data over frequency, corresponding to a spectral pair of magnitude and

25   phase shift for every 4-point-array. Figure 10 shows the data fit for the 2-D inversion of the Schilthorn measurements. The top panel (a) shows the misfit of amplitude and phase shift over the profile length. The residuals are averaged over all measurements with all configurations with the same midpoint. The total inversion misfit is $\chi = 3.4$, based on the average relative standard deviation of amplitude (0.16) and phase measurements (0.10). The inversion converged after nine iterations. The misfits of amplitude and phase are homogeneous over the profile, except around profile meter 10, where the phase misfit is significantly

30   higher. As can be seen from Fig. 7, this is the area where ρ and τ show another change for the deeper region. The higher misfit corresponds to the data of larger configurations (dipole-dipole with $n = 5, 6$), where the measured signals show slightly different curves than for the shallower measurements. The large misfit indicates that the deep structure should be treated with caution because it could be caused by difficulties in matching data.
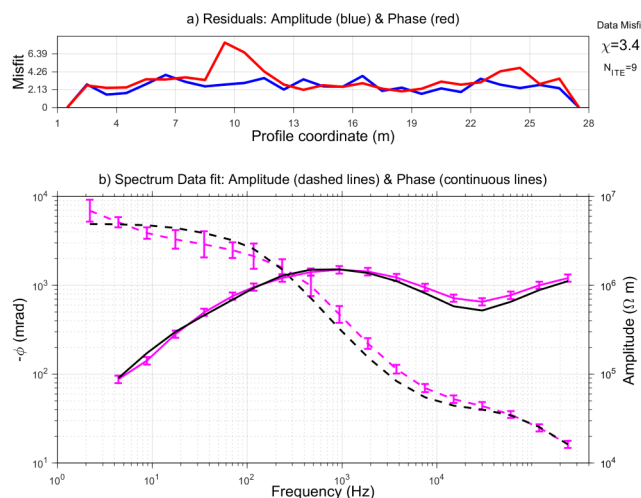
Figure 10. Data fit of the 2-D inversion of profile B-SCH. The top panel shows the misfit of amplitude (blue) and phase shift (red) over the profile. The bottom panel shows an example of measured and inverted spectra of amplitude (dashed lines) and phase (continuous lines), which belong to the dipole-dipole measurement starting from profile meter 16 ($a = 1\,\mathrm{m}$, $n = 1$) along the profile direction (see fig. 7). The measured data is the same as in figure 4, with resistivity instead of impedance, and phase shift on a logarithmic scale. The total data misfit is $\chi = 3.4$ after 9 iterations. For each profile coordinate, the misfit of all data corresponding to this point were averaged to obtain the top panel.

Panel (b) of Fig. 10 shows the data fit of the spectrum, which was previously shown during the discussion of the single site inversion (Fig. 4). Data and inversion results are shown for the amplitude (dashed lines) and the phase (continuous lines). The amplitude is not exactly the same as the magnitude in Fig. 4, but was converted to the frequency dependent resistivity (using Eq. (3)). The negative phase shift is displayed on a logarithmic scale in $mrad$. Some data points, in this case for the

5   two lowest frequencies, that caused difficulties for the inversion code and were identified as outliers, are not shown. Overall, for both amplitude and phase shift, the shape of the spectrum is well matched. For several data points, the calculated curve is not within the data errors, which is reflected in a misfit value $\chi > 1$. The data errors are calculated by the device by stacking multiple measurements. Considering that broadband electrical data of 79 spectra were matched with a single 2-D model, we find the fit satisfactory. The 19 discrete measured frequencies seem to be sufficient to define the dispersion of permittivity.

10   Another example of data spectra is shown in Fig. 11 for the measurements taken at Lake Prestvannet. The data are the same as discussed in Fig. 5, with one lake measurement (blue) and one onshore measurement (red) corresponding to profile coordinates $11.5\,\mathrm{m}$ and $28\,\mathrm{m}$ from Fig. 9. The total data misfit of the inversion is $\chi = 1.8$. The onshore spectra shows some similarity to the Schilthorn spectra (Fig. 10). The amplitude and the phase shift are both matched very well. As mentioned before for the single site inversion, the spectra of lake and land show a different frequency-dependent behaviour. A slight difference between

15   the measured and calculated data is visible for the phase of the lake measurement in the intermediate frequency range. This could indicate limitations of the single Cole-Cole model.
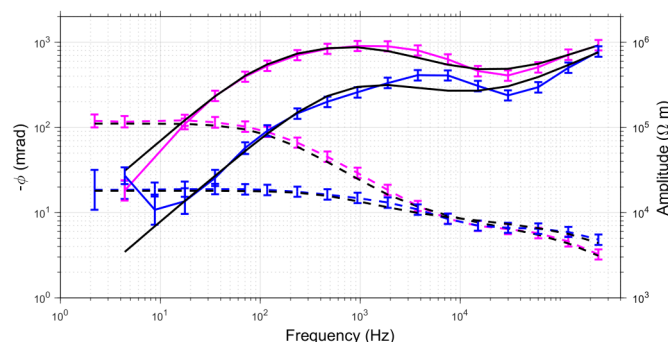
Figure 11. Data fit of the 2-D inversion for two stations of the lake Prestvannet profile. The blue lines correspond to a station at $11.5\,\mathrm{m}$, which is on the lake, the red line to a station at $28\,\mathrm{m}$, onshore. Both were measured with a Wenner configuration ($a = 1.5\,\mathrm{m}$). The measured data are the same as in figure 5. The amplitude is indicated by the dashed lines and the phase shift by the solid lines.

The sensor height effect is not negligible in this case. The lowest two frequencies seem to be affected and can not be matched by the inversion. This is the same effect as discussed previously during the single site inversion.

5 Conclusions

Wide-band complex resistivity measurements based on capacitively coupled electrodes were carried out on two cryospheric
5 field sites, on a frozen lake in Norway and in an alpine region in Switzerland. By recording the spectral data in an inter-
mediate frequency range, where conduction currents and displacement mechanisms are relevant, the determination of the
frequency-dependent electrical resistivity and permittivity is investigated. The data analysis is done by a novel 2-D inversion
for broad-band electrical measurements based on the inversion tool AarhusInv, where the permittivity is parameterized with a
Cole-Cole model.
10 The first applications of the 2-D inversion give encouraging results in the sense of consistence with known materials and struc-
ture. For our shallow field measurements, the single Cole-Cole model seems sufficient and there is no evidence of fundamental
difficulties in fitting spectral data. The observed misfits are acceptable in a sense that χ is close to 1, in the range typical for
conventional 2-D resistivity inversions, and should have similar causes, such as 3-D effects. In principle, it is possible to im-
plement a double Cole-Cole model, which could fit more complex spectra, but has more inversion parameters. The assumption
15 of zero sensor height seems to be uncritical in our chosen field applications. In some cases, it could be helpful to discard some
low-frequency data, which are most strongly affected by electrode height above the observed surface.
The determination of the electrical parameters was successful and they are reasonably consistent with literature values. The
inversion for the five Cole-Cole parameters works as well as conventional 2-D resistivity inversion, except for the frequency
exponent, which tends to show spatially incoherent images. The complementary information provided by the high- and low-
20 frequency limits of permittivity can be significant. Some structures are more clearly defined than in the corresponding resistivity

image. We conclude that using different parameter sections for the interpretation can lead to a more differentiated analysis of the subsurface.

The full spectral information can be used for the determination of ground ice content at the field scale, as suggested by Grimm and Stillman (2015). This is an objective of research in periglacial environments, and will be a subject of future work.

References

Achammer, T. and Denoth, A.: Snow dielectric properties: from DC to microwave X-band, Ann Glaciol, 19, 92 – 96, https://doi.org/10.3189/S0260305500011034, 1994.

Arenson, L., Colgan, W., and Marshall, H.: Physical, Thermal, and Mechanical Properties of Snow, Ice, and Permafrost, In: Snow and Ice-Related Hazards, Risks and Disasters, https://doi.org/10.1016/B978-0-12-394849-6.00002-0, 2015.

Auken, E., Christiansen, A., Kirkegaard, C., Fiandaca, G., Schamper, C., Behroozmand, A., Binley, A., Nielsen, E., Effersø, F., Christensen, N., Sørensen, K., Foged, N., and Vignoli, G.: An overview of a highly versatile forward and stable inverse algorithm for airborne, ground-based and borehole electromagnetic and electric data, Explor Geophys, 46, 223 – 235, https://doi.org/10.1071/EG13097, 2014.

Bitelli, M., Flury, M., and Roth, K.: Use of dielectric spectroscopy to estimate ice content in frozen porous media, Water Resour Res, 40, W04 212, https://doi.org/10.1029/2003WR002343, 2004.

Cole, K. and Cole, R.: Dispersion and Absorption in Dielectrics: 1.Alternating Current Characteristics, J Chem Phys, 9, 341 – 351, https://doi.org/10.1063/1.1750906, 1941.

Dashevsky, Y., Dashevsky, O., Filkovsky, M., and Synakh, V.: Capacitance Sounding: a New Geophysical Method for Asphalt Pavement Quality Evaluation, J Appl Geophys, 57, 95 – 106, https://doi.org/10.1016/j.jappgeo.2004.10.001, 2005.

Evans, S.: Dielectric Properties of Ice and Snow – a Review, J Glaciol, 5, 773 – 792, https://doi.org/10.3189/S0022143000018840, 1965.

Fiandaca, G.: Induction-free acquisition range in spectral time- and frequency-domain induced polarization at field scale, Geophys J Int, https://doi.org/10.1093/gji/ggy409, 2018.

Fiandaca, G., Ramm, J., Binley, A., Gazoty, A., Christiansen, A., and Auken, E.: Resolving spectral information from time domain induced polarization data through 2-D inversion, Geophys J Int, 192, 631 – 646, https://doi.org/10.1093/gji/ggs060, 2013.

Fiandaca, G., Christiansen, A., and Auken, E.: Depth of Investigation for Multi-parameters Inversions, European Association of Geoscientists and Engineers. Near Surface Geoscience 2015. Conference Paper, 631 - 646, https://doi.org/10.3997/2214-4609.201413797, 2015.

Flageul, S., Dabas, M., Thiesson, J., Reijiba, F., and Tabbagh, A.: First in situ test of a new electrostatic resistivity meter, Near Surf Geophys, 11, 265 – 273, https://doi.org/10.3997/1873-0604.2012063, 2013.

Günther, T. and Martin, T.: Spectral two-dimensional inversion of frequency-domain induced polarization data from a mining slag heap, J Appl Geophys, 135, 436 – 448, https://doi.org/10.1016/j.jappgeo.2016.01.008, 2016.

Grard, R.: A quadrupolar array for measuring the complex permittivity of the ground: application to Earth prospection and planetary exploration, Meas Sci Technol, 1, 295 – 301, 1990.

Grard, R. and Tabbagh, A.: A mobile four-electrode array and its application to the electrical survey of planetary grounds at shallow depth, J Geophys Res, 96, 4117 – 4123, https://doi.org/10.1029/90JB02329, 1991.

Grimm, R. and Stillman, D.: Field Test of Detection and Characterisation of Subsurface Ice using Broadband Spectral-Induced Polarisation, Permafrost Periglac, 26, 28 – 38, https://doi.org/10.1002/ppp.1833, 2015.

Grimm, R., Stillman, D., and MacGregor, J.: Dielectric signatures and evolution of glacier ice, J Glaciol, 61, 1159 – 1170, https://doi.org/10.3189/2015JoG15J113, 2015.

Hauck, C. and Kneisel, C.: Application of Capacitively-coupled and DC Electrical Resistivity Imaging for Mountain Permafrost Studies, Permafrost Periglac, 17, 169 – 177, https://doi.org/10.1002/ppp.555, 2006.

Hilbich, C., Hauck, C., Hoelzle, M., Scherler, M., Schudel, L., Völksch, I., Vonder Mühll, D., and Mäusbacher1, R.: Monitoring mountain permafrost evolution using electrical resistivity tomography: A 7-year study of seasonal, annual, and long-term variations at Schilthorn, Swiss Alps, J Geophys Res, 113, F01S90, https://doi.org/doi:10.1029/2007JF000799, 2008.

Hördt, A., Weidelt, P., and Przyklenk, A.: Contact impedance of grounded and capacitive electrodes, Geophys J Int, 193, 187 – 196, https://doi.org/doi:10.1093/gji/ggs091, 2013.

Imhof, M., Pierrehumbert, G., Haeberli, W., and Kienholz, H.: Permafrost Investigation in the Schilthorn Massif, Bernese Alps, Switzerland, Permafrost Periglac, 11, 189 – 206, 2000.

Kuras, O., Beamish, D., Meldrum, P., and Ogilvy, R.: Fundamentals of the capacitive resistivity technique, Geophysics, 71, No.3, 135 – 152, https://doi.org/doi:10.1190/1.2194892, 2006.

Kuras, O., Beamish, D., Meldrum, P., Ogilvy, R., and Lala, D.: Capacitive Resistivity Imaging with Towed Arrays, J Environ Eng Geoph, 12, 267 – 279, https://doi.org/10.2113/JEEG12.3.267, 2007.

Loke, M. and Barker, R.: Rapid least-squares inversion of apparent resistivity pseudosections by a quasi-Newton method, Geophys Prospect, 44, 131 – 152, https://doi.org/Rapid least-squares inversion of apparent resistivity pseudosections by a quasi-Newton method, 1996.

Madsen, L., Fiandaca, G., Auken, E., and Christiansen, A.: Time-domain induced polarization - an analysis of Cole-Cole parameter resolution and correlation using Markov Chain Monte Carlo inversion, Geophys J Int, 211, 1341 – 1353, https://doi.org/10.1093/gji/ggx355, 2017.

Maurya, P., Fiandaca, G., Christiansen, A., and Auken, E.: Field-scale comparison of frequency- and time-domain spectral induced polarization, Geophys J Int, 214, 1441 – 1466, https://doi.org/10.1093/gji/ggy218, 2018.

McNeill, J.: Electromagnetic terrain conductivity measurement at low induction numbers, Technical note TN-6, Geonics Ltd., 1980.

Militzer, H. and Weber, F.: Angewandte Geophysik,2 :Geoelektrik-Geothermik-Radiometrie-Aerogeophysik, Springer Wien, Akademie-Verlag Berlin, 1985.

Murton, J. B., Kuras, O., Krautblatter, M., Cane, T., Tschofen, D., Uhlemann, S., Schober, S., and Watson, P.: Monitoring rock frezing and thawing by novel geoelectrical and acoustic techniques, J Geophys Res-Earth, 121, 2309 – 2332, https://doi.org/10.1002/2016JF003948, 2016.

Olatinsu, O. B., Olorode, D. O., and Oyedele, K. F.: Radio frequency dielectric properties of limestone and sandstone from Ewekoro, Earstern Dahomey Basin, Advances in Applied Science Research, 4, 150 – 158, 2013.

Olhoeft, G. R.: Electrical properties of natural clay permafrost, Can J Earth Sciences, 14, 16 – 24, https://doi.org/10.1139/e77-002, 1977.

Palacky, G. J.: Resistivity characteristics of geologic targets, In: Electromagnetic methods in applied geophysics, 52 - 129, https://doi.org/10.1190/1.9781560802631.ch3, 1988.

Pelton, W., Ward, S., Hallof, P., Sill, W., and Nelson, P.: Mineral discrimination and removal of inductive coupling with multifrequency IP, Geophysics, 43, 588 – 609, https://doi.org/10.1190/1.1440839, 1978.

Petrenko, V. and Whitworth, R.: Physics of Ice, Oxford University Press, New York, 2002.

Przyklenk, A., Hördt, A., and Radić, T.: Capacitively-Coupled Resistivity measurements to determine frequency-dependent electrical parameters in periglacial environments - theoretical considerations and first field tests, Geophys J Int, 206, 1352 – 1365, https://doi.org/10.1093/gji/ggw178, 2016.

Radić, T.: First Results from the New Multi-purpose Instrument CapGeo, 19th European Meeting of Environmental and Engeneering Geophysics, Near Surface Geoscience, https://doi.org/10.3997/2214-4609.20131364, 2013.

Rowan, M.: Structural geometry of the Wildhorn Nappe between the Aar massif and the Brienzer See, Eclogae Geol Helv, 86/1, 87 – 119, 1993.

Seidensticker, K., Möhlmann, D., Apathy, I., Schmidt, W., Thiel, K., Arnold, W., Fischer, H., Kretschmer, M., Madlener, D., Peter, A., Trautner, R., and Schieke, S.: Sesame – An Experiment of the Rosetta Lander Philae: Objectives and General Design, Space Sci Rev, 128, 301 – 337, https://doi.org/10.1007/s11214-006-9118-6, 2007.

Seshadri, S., Chin, K., Buehler, M., and Anderson, R.: Using Electrical Impedance Spectroscopy to Detect Water in Planetary Regoliths, Astrobiology, 8, 781 – 792, https://doi.org/10.1089/ast.2007.0180, 2008.

Souffaché, B., Cosenza, P., Flageul, S., Pencolé, J.-P., Seladji, S., and Tabbagh, A.: Electrostatic multipole for electrical resistivity measurements at the decimetric scale, J Appl Geophys, 71, 6 – 12, https://doi.org/10.1016/j.jappgeo.2010.01.009, 2010.

Stabbel, B.: Development of the diatom flora in Prestvannet, Tromsø, northern Norway, Norsk Geol Tidsskr, 65, 179 – 186, 1985.

Stillman, D. and Grimm, R.: Low-Frequency Electrical Properties of Ice-Silicate Mixtures Regoliths, J Phys Chem-US, 114, 6065 – 6073, https://doi.org/10.1021/jp9070778, 2010.

Tabbagh, A., Hesse, A., and Grard, R.: Determination of electrical properties of the ground at shallow depth with an electrostatic quadrupole: Field trials on archaelogical sites, Geophys Prospect, 41, 579 – 597, https://doi.org/10.1111/j.1365-2478.1993.tb00872.x, 1993.

Tarasov, A. and Titov, K.: On the use of the Cole–Cole equations in spectral induced polarization, Geophys J Int, 195, 352 – 356, https://doi.org/10.1093/gji/ggt251, 2013.

Telford, W. M., Geldart, L. P., and Sheriff, R. E.: Applied Geophysics, Cambridge Univ. Press, 2. edn., textbook gravity seismics electrical-properties magnetics MT resistivity DC IP tellurics WL, 1990.

Weidelt, P.: Grundlagen der Geoelektrik, in Handbuch zur Erkundung des Untergrundes von Deponien und Altlasten, pp. 65-94, ed. Knödel, K., Krummel, H., Lange, G., Band 3: Geophysik, Springer, Berlin, 1997.

Yuval, D. and Oldenburg, W.: Computation of Cole-Cole parametes from IP data, Geophysics, 62/2, 436 – 448, https://doi.org/10.1190/1.1444154, 1997.

Zorin, N. and Ageev, D.: Electrical properties of two-component mixtures and their application to high-frequency IP exploration of permafrost, Near Surf Geophys, 15, 603 – 613, https://doi.org/10.3997/1873-0604.2017043, 2017.